Published in final edited form as:
Biomaterials. 2010 October ; 31(29): 7526–7533. doi:10.1016/j.biomaterials.2010.06.032.

Mechanism of *Escherichia coli* inactivation on palladium-modified nitrogen-doped titanium dioxide

Pinggui Wu[a,c], **James A. Imlay**[b], and **Jian Ku Shang**[a]

[a]Department of Materials Science and Engineering, University of Illinois at Urbana-Champaign, Urbana, IL 61801 USA

[b]Department of Microbiology, University of Illinois at Urbana-Champaign, Urbana, IL 61801 USA

[c]Superior Graphile Co. PRC Tech Center, Chicago, IL 60632, USA

Keywords

Antimicrobial; Titanium oxide; Cytotoxicity; SEM; TEM; Nanoindentation

1. Introduction

Infection control continues to be a growing concern of hospitals and other medical and healthcare facilities. According to the U.S. national Centers for Disease Control and Prevention (CDC), the risk of acquiring a serious infection while being treated in a hospital has risen over 35% in the last 20 years. A study released recently found that nearly 2 million American patients contract nosocomial, or hospital-acquired, infections each year. Of these patients, nearly 90,000 die each year as a result [1]. To all the medical and healthcare facilities, the need for infection control guidelines and prevention methods is keen. A scenario that shares this common concern is the occurrence of implant-associated infections; therefore, various types of modified surfaces, which are often coated or integrated with antibiotics or metal ions, have been proposed to disrupt the colonization of bacteria [2]. Even though the biocompatibility of most of these antimicrobial surfaces remains unknown, research activities on new bactericidal materials or devices never cease.

Ti-based alloys are one of the most commonly used implant materials. The oxide of Ti, titanium dioxide (TiO_2), is known to act as a photocatalyst upon irradiation with ultraviolet light. Electron-hole pairs are generated on TiO_2 surface which result in a series of photocatalytic reactions. The resultant hydroxyl radicals and superoxide ions are highly reactive with contacting organic compounds. Since the year 1985 when Matsunaga *et al.* [3] discovered the bactericidal activity of TiO_2, this wide bandgap semiconductor and its modified forms have been successfully applied as antimicrobial agents. Recent studies have reported the successful attachment of TiO_2 onto glass [4], carbon or glass fiber [5], optical fiber [6–7], metal [8], and stainless steel [9]. They are of significant importance for different applications, from the purification of air [10] and water [11–13] to the sterilization of food preparation surfaces [14], hospital gears [15], and surgical implants [8]. A recent novel application drew much attention in which TiO_2 was applied to cotton textiles which are found antibacterial while nontoxic to human dermal fibroblasts [16]. There has also been effort to use TiO_2 coated materials against bio-implant-related infections. Using ultrafine TiO_2 powders to destroy cancer cells, Cai *et al.* made one of the earliest attempts on new

Correspondence to: Jian Ku Shang.

application of TiO_2 photocatalyst for medical applications [17–18]. Since the surface of Ti-implants is a stable layer of protective titanium dioxide through air-induced passivation [2], Choi *et al.* recently conducted *in vitro* studies on the antibacterial response of titanium-made orthodontic materials under UV irradiation against *Lactobacillus acidophilus* and *Streptococcus mutans* [19–20]. Riley *et al.* reported a similar evaluation on the bactericidal effect of these materials on *E. coli* strains [21].

Nevertheless, although there are numerous publications on the bactericidal effect of TiO_2 materials upon irradiation, there have been very few thorough reports on the mechanism of this bactericidal effect. Accordingly, this work has been designed to investigate the mechanism of disinfection by TiO_2 photocatalyst. The aims of this research are twofold. First, we will evaluate the antimicrobial results of a modified TiO_2-embedded fiber material before and after being irradiated with visible-light. Second, we will give insight on the reasons for bacterial viability loss. For these purposes, we will work with strains of *E. coli* on PdO/TiON-embedded fiber.

Without exhaustive details, chemical and physical modifications to TiO_2 in recent studies have yielded a range of new photocatalysts with visible-light-induced activity [22–23]. Recently, the combination of Pd ion and nitrogen resulted in a visible-light activated PdO/TiON photocatalyst, which has shown remarkable photocatalytic activities on a wide range of organic [24], metallic [25]and microbiological species [26–29]. The addition of PdO allows the electron transfer process on the photocatalyst to be “regulated” by storing and releasing electrons to minimize electron-hole recombination [30] or to produce a long-lasting photocatalytic ‘memory’ effect after light is turned off [28 31]. While the hydroxyl radicals generated by the visible light photocatalysis are believed to be the working species in bacterial inactivation [28 31], the mechanism by which the hydroxyl radicals effect the bacterial killing on PdO/TiON photocatalyst remain unclear.

In the UV/TiO_2 system, researchers have proposed three different mechanisms of killing, including a) detrimental effects on deoxyribonucleic acid (DNA) molecules [32]; b) cell wall and cell membrane damage [33] that leads to leakage of the cell contents [34]; c) observed decrease or loss of respiratory activities due to oxidation/loss of coenzyme A [3]. Although direct evidence for photocatalytic killing is still lacking, microscopy observations have been reported of cell wall and cell membrane damage to *E. coli* [35–36]. On the other hand, a CdSe/ZnS-photosensitized nano-TiO_2 film was recently found to induce plasmid DNA damage. Since most of these observations are made long after the photocatalysis begins, the post-mortem examinations by a single technique alone cannot ascertain the mechanism of bacterial inactivation by photocatalysts.

In this study, chemical assay and several microscopic techniques were combined to characterize the cellular responses of *E. coli* to visible light photocatalysis at different treatment intervals. With these techniques, a comprehensive view of the cellular response was obtained, which not only documented the morphological changes in the cell wall and membrane but also revealed the dynamic evolution of photocatalytic damages. By relating such a comprehensive view of the photocatalytic damage process with the antimicrobial properties of PdO/TiON photocatalyst, we concluded that the photocatalytic disinfection by PdO/TiON results primarily from the oxidative attack from the exterior to the interior of the bacterium by hydroxyl radicals.

2. Materials and Methods

2.1 The photocatalyst

Our previous report on PdO/TiON-deposited fiber photocatalyst detailed the material preparation procedure [27]. A mixture of titanium tetraisopropoxide and tetramethylammonium hydroxide (mol ratio 4:1) was first made in absolute ethanol. Then a proper amount of $Pd(acac)_2$ dissolved in CH_2Cl_2 was added. Activated carbon-coated glass fiber (ACGF) was soaked in the precursor mixture for 24 h at room temperature. After wash and dry, fine crystallites of PdO/TiON nanoparticles deposited on fibers were obtained by calcination (400°C, 3 h), followed by removal of carbon at 500°C for 1 h in air.

2.2 Bacteria cell viability assay

The disinfection experimental set-up and typical *E. coli* killing kinetics [26], as well as determination of the key reactive oxygen species produced from irradiated PdO/TiON photocatalysts, were previously reported elsewhere [28]. For viability assays, a typical procedure of photocatalytic treatment is as follows. Overnight-cultivated *E. coli* AN387 was washed and resuspended in buffer solution (0.05 M KH_2PO_4 and 0.05 M K_2HPO_4, pH 7.0) to *ca.*10^9 colony-forming units per ml (cfu/ml). The cell suspension was pipetted onto a sterile petri dish which was illuminated by a visible-light source (*ca.* 1.6 mW/cm^2) in the presence of the PdO/TiON fiber photocatalyst. At regular time intervals, 20 μL aliquots of the irradiated cell suspensions were withdrawn. After appropriate dilutions in buffer, aliquots of 20 μL together with 2.5 ml top agar were spread onto agar medium plates (composition in Table 1) and incubated at 37°C for 18–24 h. The number of viable cells in terms of colony-forming units was counted. The *E. coli recA* mutant strain AS224 was used for a comparative study following the same viability assay. The hypersensitivity of AS224 mutants to DNA damage was first confirmed with in-house UV irradiation prior to use of the bacteria.

2.3 Scanning electron microscopy

Overnight grown *E. coli* was washed and resuspended in buffer solution to *ca.*10^9 cfu/ml. Cells without or with photocatalytic treatment were collected by centrifugation. The cell pellet was fixed in 2.5% glutaraldehyde for 2 h in a refrigerator. After fixation, the cell pellets were soaked in cacodylate buffer to remove excess fixative. Post-fixation processing was carried out in 1% osmium tetroxide in cacodylate buffer for 90 min at room temperature, and the pellets were then washed with cacodylate buffer. The samples were dehydrated by successive soakings in 37, 67, 95% (v/v) ethanol for 10 min each and then three soakings in 100% ethanol for 15 min each. Critical point drying was performed by placing samples in hexamethyldisilazane (HMDS) for 45 min and overnight drying under a fume hood after drawing the HMDS off. SEM images of the samples were obtained using a scanning electron microscope Hitachi S-4700 (Hitachi, Tokyo, Japan) at an acceleration voltage 5 or 10 kV.

2.4 Transmission Electron Microscopy (TEM)

Overnight-grown *E. coli* was washed and resuspended in buffer solution to *ca.*10^9 cfu/ml. Cells without or with photocatalytic treatment were collected by centrifugation. The collected *E. coli* cell pellet was processed, and TEM images were taken by specialists in the Center for Microscopic Imaging (CMI) of the College of Veterinary Medicine, University of Illinois at Urbana-Champaign. The pellet was fixed in Karnovsky's fixative at refrigerator temperatures for a minimum of 3 h until processing. Microwave techniques were used for fixation and other steps in the procedure. The sample was first washed with cacodylate buffer and secondarily fixed in 2% osmium tetroxide, followed by the addition of potassium

ferrocyanide. The sample was then washed in water and enbloc stained with uranyl acetate. The cells were dehydrated by successive incubations in 25, 50, 75, and 95% (v/v) ethanol for 8 min each, two incubations in 100% ethanol, and finally two incubations in 100% acetonitrile. The sample pellets were then infiltrated with a mixture of epoxy resin and acetonitrile (1:1 v/v) for 10 min, a mixture of epoxy resin and acetonitrile (4:1 v/v) for 20 min, and finally pure epoxy resin for 3 h at room temperature. Following infiltration, the sample was placed in individual embedding capsules, spun down to a pellet, and then polymerized at 85°C overnight. These samples were removed from the capsules and trimmed. Ultrathin sections (60–90 nm) were mounted on copper grids and stained with uranyl acetate and lead citrate. TEM images were obtained with a Hitachi H600 transmission electron microscope operated at 75 kV.

2.5 Fluorescence microscopy

A rapid epifluorescence staining method using the LIVE/DEAD® *Bac*Light™ Bacterial Viability Kit (Molecular Probes, Eugene, OR, USA) was applied to reveal the membrane damage of *E. coli* after treatment. According to the manufacturer, *Bac*Light is composed of two nucleic acid-binding stains: SYTO 9™ and propidium iodide. SYTO 9™ penetrates all bacterial membranes and stains the cells green, while propidium iodide only penetrates cells with damaged membranes. The combination of the two stains produces red fluorescing cells. The procedure followed the method previously described [37]. The two *Bac*Light stains, SYTO 9 and propidium iodide, were dissolved in DMSO, mixed together (300 μL+300 μL), and diluted 1:10 in a NaCl solution (0.085%), providing 6 ml of *Bac*Light stock solution. The stock solution was kept at −20°C and protected from light. When needed, a volume of 30 μl of *Bac*Light was added to 1 ml of sample. Samples were incubated in the dark at room temperature for 20 min. After incubation, the stained sample was filtered through a 0.2-μm Nuclepore black polycarbonate filter. The filter was then placed on a slide between two drops of low fluorescence immersion oil (Cargille type DF), mounted in *Bac*Light mounting oil as described in the manual provided by the manufacturer, and covered with a clear glass cover slip. At Backman Research Institute (UIUC), a Zeiss Axiovert 100 inverted research-grade microscope was configured to perform fluorescence microscopy. An AttoArc HBO 100W mercury lamp was used as the light source, and a 480-nm excitation filter was used. Images were obtained using a 100× oil immersion lens, recorded through a Hammamatsu CCD camera.

2.6 Atomic force microscopy

Bacteria were attached through electrostatic interactions (physical adsorption) to a wafer slide that had been positively charged by adsorption of poly-L-lysine hydrobromide. For coating of the slide surface with poly-L-lysine hydrobromide (Sigma-Aldrich P0879, mol. wt 1,000–4,000), these procedures were followed [38]. The wafer was cleaned by sonication for 30 min in 1 M HCl (= 86.2 ml in 1 liter), rinsed thoroughly with deionized water, dipped in methanol, and rinsed again with deionized water to remove any debris and to uniformly wet the surface of the slide. Each wafer slide was placed into into a clean 40 mL-beaker. The slide was then incubated for 30–60 min in sufficient 0.01% (wt/vol) poly-L-lysine hydrobromide solution in 0.085% NaCl saline to completely cover the surface of the wafer slide. The slide was then washed thoroughly with 0.085% NaCl saline to remove any excess poly-L-lysine, which appears to be very toxic to cells. Slides were then allowed to dry completely while being covered so that nothing stuck to the slide. After air-drying, the slide was rinsed with deionized water and dipped into the bacterial suspension in water. After 15 min, the bacteria-attached slide was rinsed with deionized water to remove loosely attached bacteria and was then immediately transferred to the AFM for observation. The AFM instruments used include both Multimode AFM of Digital Instruments/Veeco and MFP-3D AFM of Asylum Research. An important application of the atomic force microscope is in

quantitative force measurements, a prerequisite of which is accurate knowledge of the cantilever spring constant. Calibration of the AFM cantilever was performed with the thermal noise method in the software.

3. Results

3.1 Quantification of the bactericidal effect

The effect of the photocatalyst on the viability of *E. coli* strains was studied by the plating assay. We have previously reported the bactericidal effect of PdO/TiON-glass fiber material to a starting ~10^7 cfu/ml cell population [26]. In the present study it started at *ca.*10^9 cfu/ml cell population. Figure 1 shows that PdO/TiON treatment resulted in *E. coli* AN387 survival ratio of ~80% after 5-min treatment, and ~10% survival ratio upon 30 min irradiation. A steep curve of disinfection was observed after the initial 30 min, with *ca.* 10^{-4} surviving at 1-h irradiation, and $<10^{-8}$ survival ratio upon 90 min treatment which indicates a complete killing. A similar killing trend was observed in Figure 1 for the disinfection of the *E. coli recA* mutant strain AS224. The two killing curves are comparable.

3.2 Indication of Membrane Damage

As mentioned earlier, the LIVE/DEAD® *Bac*Light™ kit can indicate the membrane damage through the color of stained cells under fluorescence microscopy [37]. Fluorescent images of *E. coli* cells prior to and after photocatalytic treatment are presented in Figures 2(a) and (b), respectively. It can be seen that the control cells prior to treatment are all stained green by the LIVE/DEAD® *Bac*Light™ kit. These cells are viable, as shown by the plating assay. Complete disinfection of the 10^9 cfu/ml cell population was normally achieved when illumination time was >1 h. Such photocatalytically treated cells in the fluorescent image of Figure 2(b) are all red. *Bac*Light™ is composed of two stains, of which propidium iodide only penetrates cells with damaged membranes, staining the cells red. The observation of red cells indicates that their membranes were damaged during photocatalytic treatment. When the duration of treatment was 30 min, 90% of the cells failed to form colonies. Fluorescent images revealed a mixture of both red and green cells (Figure 2c). Thus after 30-min photocatalytic disinfection treatment, some cells retain intact membranes, while others do not.

3.3 Observation of Membrane Damage

SEM and TEM are suitable tools for investigation of morphology and microstructure of bacteria cells. Figure 3(a) shows a representative SEM image of *E. coli* cells before photosterilization treatment. In this control sample, the surfaces of rodlike bacteria are smooth and damage-free. It indicates that the cells were healthy before they were treated with PdO/TiON photocatalyst. However, after complete disinfection of the bacteria cells under visible-light illumination for 2 h in the presence of PdO/TiON photocatalyst, the morphologies of cells showed drastic changes. First, flagella which were observed in untreated cells were completely missing in Figures 3(b) and (c) of treated cells. Second, in nearly every cell, the appearance of rumples and a high degree of disconfigurations were observed. Images in Figures 3(b) and (c) show that many *E. coli* cells were missing parts of the cell wall and the cell membrane or even material inside, so that deep ‘holes’ appeared. These images obtained in two separate sets of experiments verified that photocatalysis caused oxidative damages on bacteria. The formation of rumples/holes in *E. coli* was in good agreement with some previous reports [35].

It is interesting to note that after treatment for 30 min (with ~90% cell population “destroyed” as indicated by the viability assay), the cell morphology and its surface structure changed little, as shown in Figure 3(d). Therefore, a mistaken conclusion of no cell wall or

cell membrane damage is easily reached if the conclusion is solely based on this morphological observation. More results will follow to show that at this disinfection stage, when bacteria cells had just lost their viability, the exterior damage in morphology has occurred; yet the damage was too subtle to be observed under SEM.

TEM images concurred with the previous SEM observation of membrane damage. Figure 4(a) is a representative TEM image of untreated *E. coli* cells that have a fluffy boundary. The fluffy outer layer is considered to be the outer membrane of *E. coli* cell. It can be noted that after photocatalytic disinfection, the outer membrane was completely decomposed. In Figures 4(b)–(d) after treatment for 2 h, a noteworthy difference from the untreated sample is that every treated cell has lost its outer membrane, i.e., the fluffy boundary. Some treated cells show a clearly-cut edge, which indicates that the plasma membrane may have been exposed after the outer membrane had decomposed. The other cells completely or partially lost this edge, which is a severely damaged stage with plasma membrane also gone. An extensively damaged ′ghost′ cell is apparent in the center of Figure 4(b). There remains no more cell wall or cell membrane in this cell; instead, many dark granules appear. The damage to the cell wall and the cell membrane observed in TEM are in good agreement with the SEM results.

3.4 Observation of Interior Damage

TEM images also show remarkable interior damage of the cells after photocatalytic disinfection. Normal *E. coli* cells exhibit a homogeneous microstructure in Figure 4(a). This image shows that a healthy *E. coli* cell has a well-defined cell wall and a uniform interior material distribution, which corresponds to an inner zone full of proteins and DNA molecules [39–40]. In contrast, dark mass aggregates appeared in the 2-h well treated cells in Figures 4(b) to (d). In some more severely compromised cells in Figures 4(c) and (d), white center regions were observed.

TEM images of an intermediate killing stage, after treatment for 30 min, are shown as Figures 5(a) to (c). Many cells still have a fluffy outer boundary, similar to that in control cells. However, a remarkable material-light center tended to be formed in the *E. coli* cells. In Figure 5(a) some substances are visible within the material-light region, in contrast to the pure-white regions of Figures 4(c) and (d). These “struggling” substances were coiled or twisted, like fingerprints. There were also some electron-dense granules/mass aggregates near the cell wall and membrane boundaries. In Figure 5(c), an *E. coli* cell was more severely damaged, as its outer membrane seemed to be decomposed (lacking the fluffy edge) and its inner structure badly disturbed. A few individual cells appeared less damaged, except for a few material-dense dark granules. It is reasonable that cells in the same batch could be subject to different degrees of photocatalytic damage.

3.5 Probe of Membrane Damage

Atomic force microscopy has been used previously in cell-substrate interaction studies [38]. In the present report, AFM provides information not only on the morphology of cells but also on the mechanical property of the cell surface, based on force measurements. A conventional thermal noise method was adopted to calibrate the cantilever and yielded a spring constant of the cantilever to be 34.5 N/m. Figure 6(a) is the AFM image of a healthy *E. coli* cell. Figure 6(b) presents a well-treated *E. coli* cell which shows a severely disrupted morphology. The force measurements were directed to each random site of interest, as marked with numbers. One force curve is shown in Figure 7, and more force curves are available in the Supplementary Data. The value of (surface) stiffness can be readily calculated from the slope of each force curve. A comparison of the values in Figure 8 shows a clear pattern: the surface of the healthy bacterium is ‘harder,’ with each stiffness value

higher than that of the damaged bacterium. Although the methodology is quantitative, a qualitative interpretation may be more reasonable. The general tendency clearly shows that the surface layer on the well-treated cell is mechanically softer than the untreated cell. The softness may be related with the loss of outer membrane as observed in SEM and TEM images, as well as related with damage to the peptidoglycan and other cellular components.

4. Discussion

4.1 The antimicrobial effect

Throughout the above results, there is no doubt on the bactericidal effect of PdO/TiON upon visible-light excitation. *E. coli* is Gram-negative bacilli responsible for many urinary tract infections. Other infectious diseases caused by *E. coli* include wound infections, neonatal meningitis, inflammation of abdominal wall, bacteremia and pneumonia [1]. The anti-bacterial results suggest the potential use of PdO/TiON for reducing the risk of infections. Furthermore, PdO/TiON photocatalyst has shown antimicrobial effect on virus [29], other Gram-negative bacteria strains of *Pseudomonas aeruginosa* [5 26], Gram-positive strains *Staphylococcus aureus* [26], and the *Bacillus subtilis* spores [27].

Traditional TiO_2 material is effective only upon UV-irradiation at intensities that would induce severe damage to human cells. A modified metal-ion and non-metal co-doped TiO_2 photocatalyst such as this PdO/TiON not only responds to visible-light illumination but also acts at rather fast rates, which makes it a better candidate than pure TiO_2 to be considered in implanted biomaterials. Within recent years different groups have tried to find some ways of using TiO_2 photocatalysis in the bio-implant field. Shiraishi *et al.* [8] reported the viability of *Staphylococcus aureus* strains against two different TiO_2 coated materials under UV irradiation. Cheng *et al.* developed some carbon-containing TiO_2 nanoparticles for bactericidal effect on several select bacteria strains under visible-light illumination [41]. The study conducted by Cushnie *et al.* [42] showed the influence of different variables on the TiO_2 antimicrobial properties using some bacteria of clinical interest. Although the biocompatibility of most of these anti-infective materials needs to be clarified, these pioneering works gave insight on future clinical studies for PdO/TiON-based antimicrobial materials to be used in fighting infection.

4.2 Mechanisms underlying the antimicrobial effect

In TEM, the appearance of apparently clear, white-color areas may result from several possible events. One could interpret the white areas to be aggregated DNA molecules [40]. It is fair to conjecture that the gross morphology of the DNA may have changed, meaning that its higher-order organization may have been disrupted upon the impact of photocatalysis, such as reported elsewhere [32 40]. Another interpretation of the phenomenon is the leaking of interior components after rupture of the cell membrane [39]. Yet another explanation might be the decomposition of interior components upon oxidation by reactive oxygen species. Although evidence should be sought to provide a solid answer, the first interpretation is more likely to be the case than the others. As reported elsewhere [28 43], the reactive oxygen species generated in the present experimental set-up are mainly hydroxyl radicals. They are known to be too reactive to diffuse the long distance through the compromised cell wall/cell membrane so that they might reach the cell center. Furthermore, if leaking or decomposition of the interior components occurs, it is more likely to start with the border areas near the cell membrane, not the center. The areas surrounding the cell membrane shall suffer the most severe consequences, not the center.

In the literature, membrane damage and DNA damage are presented as the two major theories of the mechanism of photocatalytic killing of bacteria. The images-based results

above did not distinguish which damage occurs first to cause the disinfection of *E. coli*. It was reported previously that *E. coli* cells filament as a consequence of the SOS response to DNA damage [44]. The SOS response is a post-replication DNA repair system that allows DNA replication to bypass lesions or errors in the DNA. The SOS uses the RecA protein. The RecA protein, stimulated by single-stranded DNA, is involved in the inactivation of the LexA repressor thereby inducing the response. Cells will form long filaments when they are stressed to the point of death through DNA damage/cell division defects, while their metabolism still functions. The common disinfectants of UV irradiation and hydrogen peroxide result in filamentation of certain bacteria, including *E. coli* [44–45]. In the present visible-light-activated photocatalytic treatment, *E. coli* cells did not exhibit the phenomenon of filamentation. In experiments for a ~80% survival ratio of the 10^9 cfu/ml cell population after 5-min treatment, not a single cell was observed to form long filament after 8-h post-treatment incubation in LB (composition see Table 1) nutrient media (Supplementary Data). The results indicate that at the death point of *E. coli* cells, they have already lost their normal metabolism activity (which could be due to membrane damage).

Although *recA* mutants are hypersensitive to all known types of DNA damage, they were not unusually sensitive to visible-light-induced photocatalysis. Data in Figure 1 indicate that the disinfection behaviors of AN387 and AS224 are similar. This result clearly shows that DNA damage is not the initial mechanism of killing during PdO/TiON photocatalytic treatment. If DNA damage were the first-step cause of disinfection, a steep rapid killing-curve for the *rec*A mutant AS224 is expected [44]. On the other hand, Figure 1 indicates the dose-response kinetics. On the semilog plot the killing curve has an obvious shoulder. A shoulder is typically observed when multiple damage events are necessary to kill a cell, such as when a membrane has to be destroyed. In contrast, DNA damage usually leads to killing without much of a shoulder [44].

It has long been a difficult task to specify the sequence of membrane damage and interior alteration in former studies on the bactericidal reactions of TiO_2. That is, the two events seem to occur close together in time, making it hard to know which event may cause death. Our presented results suggest that the delicate cell membrane is subject to oxidative damage first by the very reactive hydroxyl radicals. The initial membrane damage is so subtle that it is not detectable in SEM and TEM until the damage advances to a greater level. But as soon as the cell's first line of defense (which is the cell wall and membrane) is broken, some interior substances (including the sensitive DNA molecules) were damaged almost immediately, and readily observable in TEM. And later both TEM and SEM clearly detect the damages. In the microbiology field, the work of Yatvin *et al.* [46] shows that the physical state of the membrane during irradiation of the cell strongly influences survival. Disruption of membrane integrity can irreversibly de-energize cells and release essential metabolites.

5. Conclusions

The mechanisms by which the visible-light-induced photocatalytic activity of PdO/TiON nanoparticulate-embedded fiber kills bacteria are suggested to be initial oxidative lesions to the cell wall and the cell membrane, followed by damage to the interior DNA molecules, eventually causing severe morphological and structural injuries to the cells.

Supplementary Material

Refer to Web version on PubMed Central for supplementary material.

Acknowledgments

P. Wu thanks Lou Ann Miller for TEM assistance. This work is supported by the Center of Advanced Materials for the Purification of Water with Systems, National Science Foundation, under Agreement Number CTS-0120978. SEM and AFM were carried out at the Frederick Seitz Materials Research Laboratory, University of Illinois at Urbana-Champaign, which is partially supported by the U.S. Department of Energy under grant DEFG02-91-ER45439.

Appendix

More AFM force-displacement curves and microscopic *E. coli* images are available as Supplementary Data. Some figures in this article have parts that are difficult to interpret in black and white. The full color images can be found in the on-line version, at doi:

References

1. Jarvis WR. Selected aspects of the socioeconomic impact of nosocomial infections: Morbidity, mortality, cost, and prevention. Infect Control Hosp Epidemiol 1996;17:552–557. [PubMed: 8875302]
2. Gallardo-Moreno A, Pacha-Olivenza M, Fernández-Calderónb MC, Pérez-Giraldo C, Bruque J, González-Martín ML. Bactericidal behavior of Ti6Al4V surfaces after exposure to UV-C light Biomater 2010;31:5159–5168.
3. Matsunaga T, Tomoda TR, Nakajima T, Wake H. Photoelectrochemical sterilization of microbial cells by semiconductor powders. FEMS Microbiol Lett 1985;29:211–214.
4. Page K, Palgrave RG, Parkin IP, Wilson M, Savin S, Chadwick AV. Titania and silver-titania composite films on glass-potent antimicrobial coatings. J Mater Chem 2007;17:95–104.
5. Wu, PG.; Xie, R.; Imlay, J.; Shang, JK. Visible-light photocatalytic fibers for inactivation of *Pseudomonas aeruginosa*. In: Wereszczak, Andrew; Lara-Curzio, Edgar; Mizuno, M., editors. Advances in bioceramics and biocomposites II, Ceramic Eng. Sci. Proc. New York: Wiley-American Ceramic Society; 2006. p. 125-128.
6. Yu MJ, Kim BW. Photocatalytic cell disruption of *Giardia lamblia* in a UV/TiO_2 immobilized optical-fiber reactor. J Microbiol Biotechnol 2004;14:1105–1113.
7. Matsunaga T, Okochi M. TiO_2-mediated photochemical disinfection of *Escherichia-coli* using optical fibers. Environ Sci Technol 1995;29:501–505.
8. Shiraishi K, Koseki H, Tsurumoto T, Baba K, Naito M, Nakayama K, et al. Antibacterial metal implant with a TiO_2-conferred photocatalytic bactericidal effect against *Staphylococcus aureus*. Surf Interface Anal 2009;41:17–22.
9. Yu JC, Ho WK, Lin J, Yip KY, Wong PK. Photocatalytic activity, antibacterial effect, and photoinduced hydrophilicity of TiO_2 films coated on a stainless steel substrate. Environ Sci Technol 2003;37:2296–2301. [PubMed: 12785540]
10. Keller V, Keller N, Ledoux MJ, Lett MC. Biological agent inactivation in a flowing air stream by photocatalysis. Chem Comm 2005:2918–2920. [PubMed: 15957025]
11. Armon RW-C, G Bettane P. Disinfection of *Bacillus spp*. spores in drinking water by TiO_2 photocatalysis as a model for bacillus anthracis. Water Sci Technol: Water Supply 2004;4:7–14.
12. Dillert R, Siemon U, Bahnemann D. Photocatalytic disinfection of municipal wastewater. Chem Eng Technol 1998;21 356-+
13. Wei C, Lin WY, Zainal Z, Williams NE, Zhu K, Kruzic AP, et al. Bactericidal activity of TiO_2 photocatalyst in aqueous-media - toward a solar-assisted water disinfection system. Environ Sci Technol 1994;28:934–938.
14. Kim B, Kim D, Cho D, Cho S. Bactericidal effect of TiO_2 photocatalyst on selected food-borne pathogenic bacteria. Chemosphere 2003;52:277–281. [PubMed: 12729712]
15. Stoimenov, P.; Klabunde, KJ. Nanotechnology in biological agent decontamination. New York: Wiley-VCH; 2005.

16. Kangwansupanonkon W, Lauruengtana V, Surassmo S, Ruktanonchai U. Antibacterial effect of apatite-coated titanium dioxide for textile applications. Nanomedicine 2009;5:240–249. [PubMed: 19223243]
17. Cai R, Hashimoto K, Itoh K, Kubota Y, Fujishima A. Photokilling of malignant cells with ultrafine TiO_2 powder. Bull Chem Soc Jpn 1991;64:1268–1273.
18. Cai R, Hashimoto K, Itoh K, Fujishima A, Kubota Y. Photocatalytic effect on tumor cells. Photomed Photobiol 1988;10:253–255.
19. Choi JY, Chung CJ, Oh KT, Choi YJ, Kim KN. Photocatalytic antibacterial effect of TiO_2 film on TiAg on *Streptococcus* mutans. Angle Orthod 2009;79:528–532. [PubMed: 19413372]
20. Choi JY, Kim KH, Choy KC, Oh KT, Kim KN. Photocatalytic antibacterial effect of TiO_2 film formed on Ti and TiAg exposed to *Lactobacillus acidophilus*. J Biomed Mater Res Pt B Appl Biomater 2007;80:353–359.
21. Riley DJ, Bavastrello V, Covani U, Barone A, Nicolini C. An *in-vitro* study of the sterilization of titanium dental implants using low intensity UV-radiation. Dent Mater 2005;21:756–760. [PubMed: 15878616]
22. Khan S, Al-Shahry M, Ingler W. Efficient photochemical water splitting by a chemically modified n- TiO_2 Science 2002;297:2243–2245.
23. Asahi R, Morikawa T, Ohwaki T, Aoki K, Taga K. Visible-light photocatalysis in nitrogen-doped titanium oxides. Science 2001;293:269–271. [PubMed: 11452117]
24. Li Q, Xie R, Mintz EA, Shang JK. Enhanced visible-light photocatalytic degradation of humic acid by palladium-modified nitrogen-doped titanium oxide. J Am Ceram Soc 2007;90:3863–3868.
25. Li Q, Easter NJ, Shang JK. As(III) removal by palladium-modified nitrogen-doped titanium oxide nanoparticle photocatalyst. Environ Sci Technol 2009;43:1534–1539. [PubMed: 19350931]
26. Wu P, Xie R, Imlay JA, Shang JK. Visible-light-induced photocatalytic inactivation of bacteria by composite photocatalysts of palladium oxide and nitrogen-doped titanium oxide. Appl Catal B: Environ 2009;88:576–581.
27. Wu P, Xie R, Shang JK. Enhanced visible-light photocatalytic disinfection of bacterial spores by palladium-modified nitrogen-doped titanium oxide. J Am Ceram Soc 2008;91:2957–2962.
28. Li Q, LY W, Wu P, Xie R, Shang JK. Palladium oxide nanoparticles on nitrogen-doped titanium oxide: Accelerated photocatalytic disinfection and post-illumination catalytic "Memory". Adv Mater 2008;20:3717–3723.
29. Li Q, Page MA, Marinas BJ, Shang JK. Treatment of coliphage MS2 with palladium-modified nitrogen-doped titanium oxide photocatalyst illuminated by visible light. Environ Sci Technol 2008;41:6148–6153. [PubMed: 18767679]
30. Li Q, Liang W, Shang JK. Enhanced visible-light absorption from pdo nanoparticles in nitrogen-doped titanium oxide thin films. Appl Phys Lett 2007;90 063109-3.
31. Li Q, Li YW, Liu ZQ, Xie RC, Shang JK. Memory antibacterial effect from photoelectron transfer between nanoparticles and visible light photocatalyst. J Mater Chem 2010;20:1068–1072.
32. Hirakawa K, Mori M, Yoshida M, Oikawa S, Kawanishi S. Photo-irradiated titanium dioxide catalyzes site specific DNA damage via generation of hydrogen peroxide. Free Radical Res 2004;38:439–447. [PubMed: 15293551]
33. Saito T, Iwase T, Horie J, Morioka T. Mode of photocatalytic bactericidal action of powdered semiconductor TiO_2 on mutans *Streptococci*. J Photochem Photobiol B: Biol 1992;14:369–379.
34. Kiwi J, Nadtochenko V. Evidence for the mechanism of photocatalytic degradation of the bacterial wall membrane at the TiO_2 interface by ATR-FTIR and laser kinetic spectroscopy. Langmuir 2005;21:4631–4641. [PubMed: 16032882]
35. Lu ZX, Zhou L, Zhang ZL, Shi WL, Xie ZX, Xie HY, et al. Cell damage induced by photocatalysis of TiO_2 thin films. Langmuir 2003;19:8765–8768.
36. Sunada K, Watanabe T, Hashimoto K. Studies on photokilling of bacteria on TiO_2 thin film. J Photochem Photobiol A 2003;156:227–233.
37. Boulos L, Prevost M, Barbeau B, Coallier J, Desjardins R. Live/dead baclighttm: Application of a new rapid staining method for direct enumeration of viable and total bacteria in drinking water. J Microbiol Methods 1999;37:77–86. [PubMed: 10395466]

38. Vadillo-Rodrigues V, Busscher HJ, Norde W, De Vries J, Dijkstra RJB, Stokroos I, et al. Comparision of atomic force microscopy interaction forces between bacteria and silicon nitride substrata for three commonly used immobilization methods. Appl Environ Microbiol 2004;70:5441–5446. [PubMed: 15345431]
39. Hu C, Lan YQ, Qu JH, Hu XX, Wang AM. Ag/AgBr/ TiO_2 visible light photocatalyst for destruction of azodyes and bacteria. J Phys Chem B 2006;110:4066–4072. [PubMed: 16509698]
40. Feng QL, Wu J, Chen GQ, Cui FZ, Kim TN, Kim JO. A mechanistic study of the antibacterial effect of silver ions on *Escherichia coli* and *Staphylococcus aureus*. J Biomed Mater Res A 2000;52:662–668.
41. Cheng CL, Sun CS, Chu WC, Tseng YH, Ho HC, Wang JB, et al. The effects of the bacterial interaction with visible-light responsive titania photocatalyst on the bactericidal performance. J Biomed Sci 2009;16:7–17. [PubMed: 19272171]
42. Cushnie T, Robertson P, Officer S, Pollard P, McCullagh C, Robertson J. Variables to be considered when assessing the photocatalytic destruction of bacterial pathogens. Chemosphere 2009;74:1374–1378. [PubMed: 19101016]
43. Li Q, Wu PG, Xie RC, Shang JK. Enhanced photocatalytic disinfection of microorganisms by transition-metal-ion-modification of nitrogen-doped titanium oxide. J Mater Res 2010;25:167–176.
44. Imlay JA, Linn S. Mutagenesis and stress responses induced in *Escherichia coli* by hydrogen peroxide. J Bacteriol 1987;169:2967–2976. [PubMed: 3298208]
45. Park S, You XJ, Imlay JA. Substantial DNA damage from submicromolar intracellular hydrogen peroxide detected in Hpx- mutants of *Escherichia coli*. Proc Natl Acad Sci USA 2005;102:9317–9322. [PubMed: 15967999]
46. Yatvin M. Evidence that survival of gamma-irradiated *Escherichia coli* is influenced by membrane fluidity. Intl J Radiation Biol 1976;30:571–575.

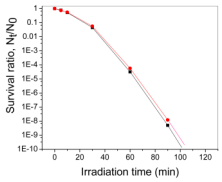

Figure 1.
The killing curves of normal *E. coli* strain AN 387 (red circles) and the *recA* mutant AS 224 (black squares) on PdO/TiON under visible light irradiation. (Note: the lines merely guide the eyes.)

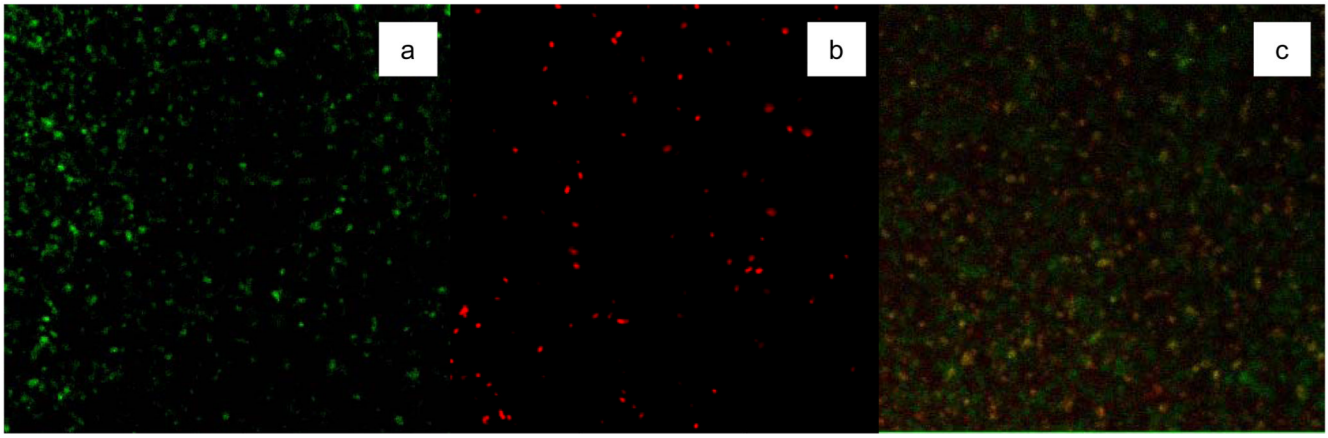

Figure 2.
E. coli viability as detected by SYTO 9™ and propidium (a) untreated, green cells are viable; (b) after photocatalytic treatment for 2-h; (c) after photocatalytic treatment for 30 min.

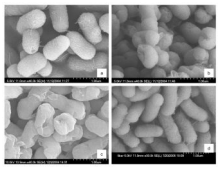

Figure 3.
SEM images of *E. coli* cells (a) untreated; (b) and (c) after photocatalytic inactivation treatment for 2-h; and, (d) after photocatalytic inactivation treatment for 30 min.

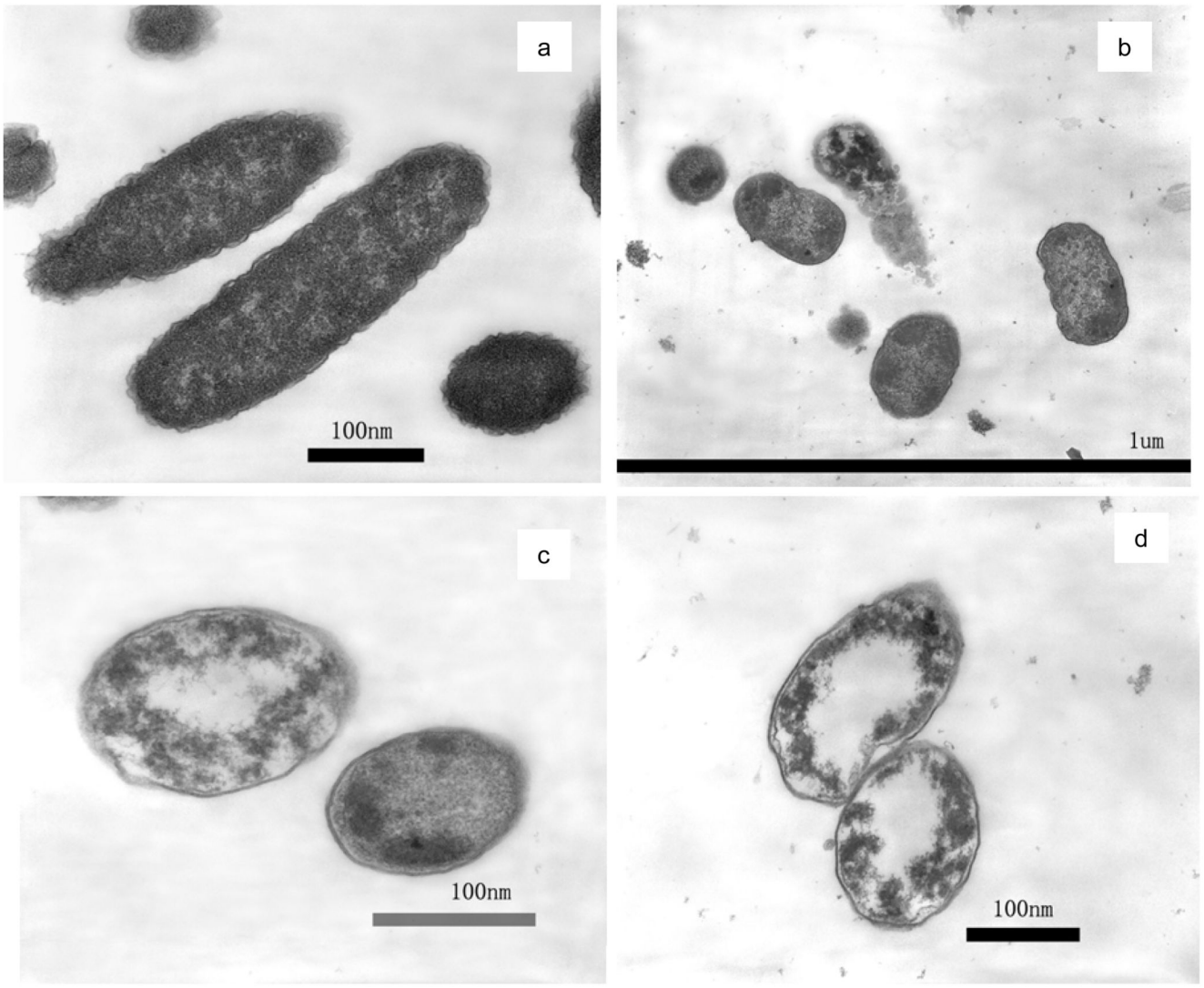

Figure 4.
TEM images of *E. coli* (a) untreated; (b), (c), and (d) after photocatalytic inactivation treatment for 2-h.

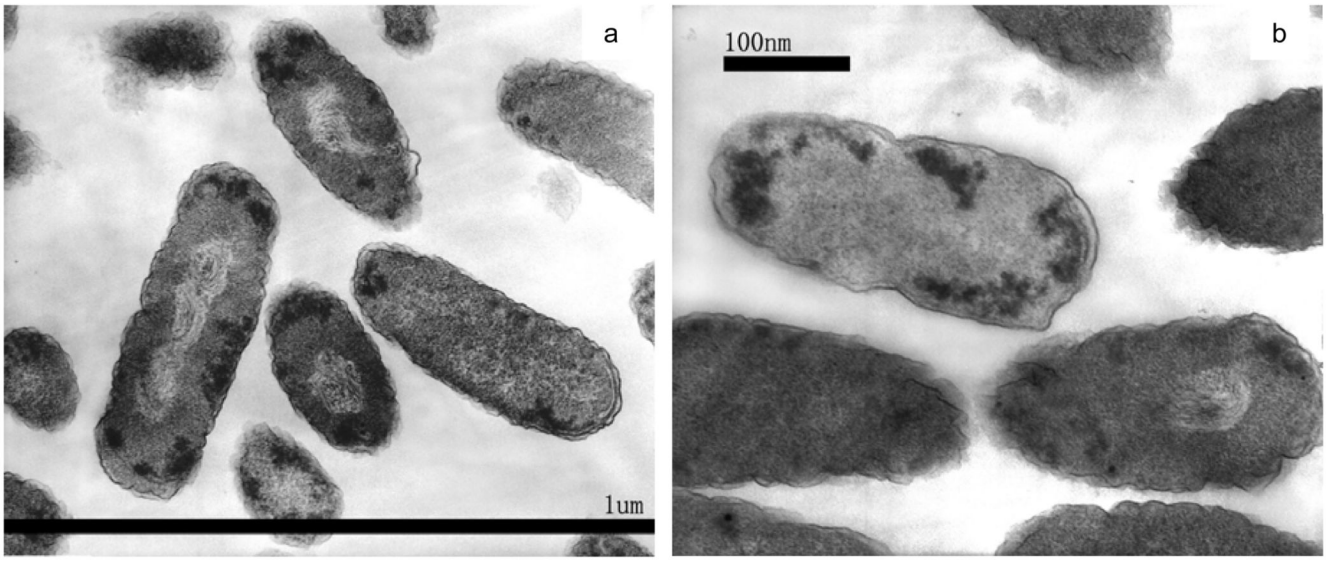

Figure 5.
TEM images of *E. coli* cells after photocatalytic inactivation treatment for 30 min.

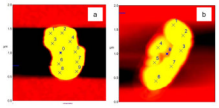

Figure 6.
AFM images of *E. coli* cells (a) untreated; and, (b) after photocatalytic treatment. (Note: marked sites for force probing.)

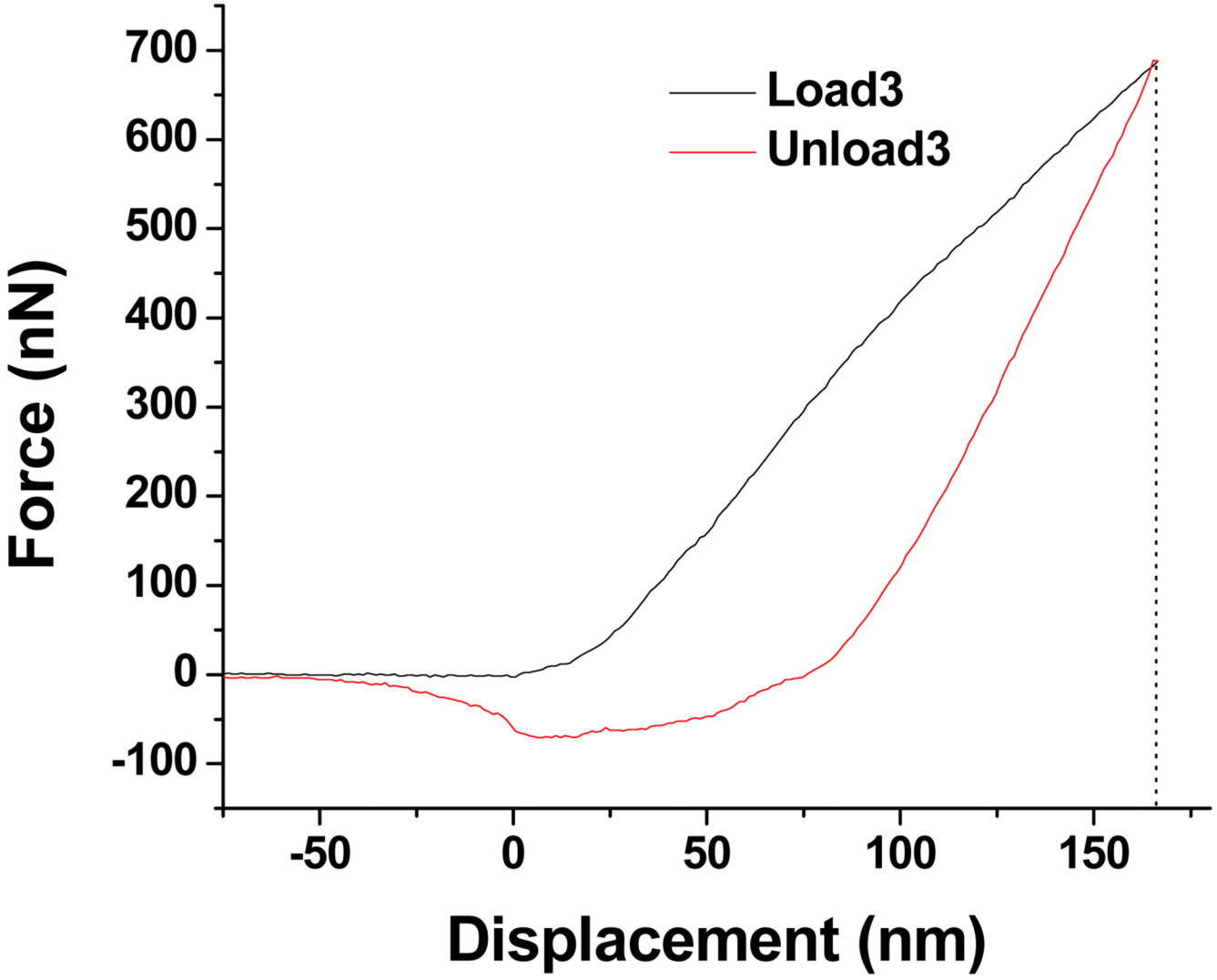

Figure 7.
Representative load-displacement curve obtained from AFM nanoindentation and force measurement on Site 3 as marked in Figure 6(b).

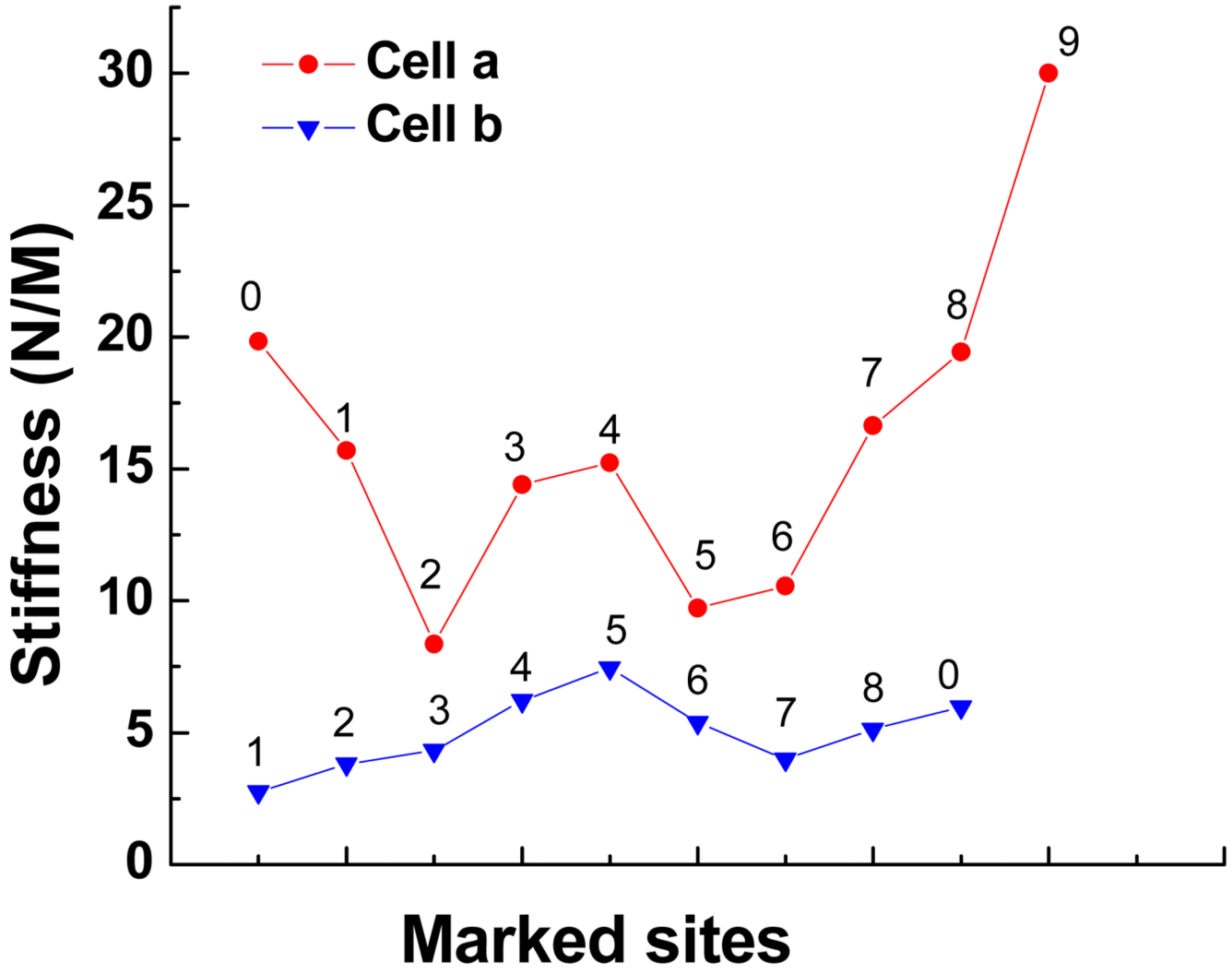

Figure 8.
Comparison of stiffness values obtained for the healthy cell in Figure 6(a) and the damaged cell in Figure 6(b).

Table 1

Media Composition (per liter)

Liquid LB medium (pH=7.0)	10 g bactotryptone + 5 g yeast extract +10 g NaCl
Medium for plating	Liquid medium + additional 15 g bactoagar
Top agar	Liquid medium + additional 8 g bactoagar